

An hybrid approach to CMB lensing reconstruction on all-sky intensity maps

S. Plaszczynski¹, A. Lavabre¹, L. Perotto², and J.-L. Starck³

¹ Laboratoire de l'Accélérateur Linéaire (LAL), CNRS : UMR8607, IN2P3, Université Paris-Sud, Orsay, France
e-mail: plaszczy@lal.in2p3.fr, lavabre@lal.in2p3.fr

² Laboratoire de Physique Subatomique et de Cosmologie (LPSC), CNRS : UMR5821, IN2P3, Université Joseph Fourier - Grenoble I, Institut Polytechnique de Grenoble, France
e-mail: perotto@lpsc.in2p3.fr

³ Laboratoire AIM (UMR 7158), CEA/DSM-CNRS-Université Paris Diderot, IRFU, SEDI-SAP, Service d'Astrophysique, Centre de Saclay, F-91191 Gif-Sur-Yvette cedex, France
e-mail: jstarck@cea.fr

Received June 15, 2022

ABSTRACT

Based on realistic simulations, we propose an hybrid method to reconstruct the lensing potential power spectrum, directly on PLANCK-like CMB frequency maps. It implies using a large galactic mask and dealing with a strong inhomogeneous noise. For $\ell \lesssim 100$, we show that a full-sky inpainting method, already described in a previous work, still allows a minimal variance reconstruction, with a bias that must be accounted for by a Monte-Carlo method, but that does not couple to the deflection field. For $\ell \gtrsim 100$ we develop a method based on tiling the cut-sky with local $10^\circ \times 10^\circ$ overlapping tangent planes (referred to in the following as *patches*). It requires to solve various issues concerning their size/position, non-periodic boundaries and irregularly sampled data after the sphere-to-plane projection. We show how the leading noise term of the quadratic lensing estimator applied onto an apodized patch can still be taken directly from the data. To not loose spatial accuracy, we developed a tool that allows the fast determination of the complex Fourier series coefficients from a bi-dimensional irregularly sampled dataset, without performing an interpolation. We show that the multi-patch approach allows the lensing power spectrum reconstruction with a very small bias, thanks to avoiding the galactic mask and lowering the noise inhomogeneities, while still having almost a minimal variance. The data quality can be assessed at each stage and simple bi-dimensional spectra build, which allows the control of local systematic errors.

Key words. Cosmic microwave background – Gravitational lensing Large-scale structure of Universe – Methods: statistical

Introduction

Experiments have now reached the sensitivity, both in resolution and noise, to detect the tiny deflection of the CMB photons ($\sigma_d \simeq 2.7'$) by the irregular distribution of matter, in their journey from the last scattering surface to us. First results on the power spectrum of this deflection field have been reported by the ACT collaboration (Das et al. 2011), and the forthcoming SPT and PLANCK data should provide firm measurements. This information gives access to a new cosmological observable, sensitive to an epoch ($1 \lesssim z \lesssim 3$) much more recent than the CMB decoupling one ($z \simeq 1100$), giving us a lever-arm to lift the so-called *geometrical degeneracy* (Stompor & Efstathiou 1999), still using one single consistent data-set. In particular it probes the matter density fluctuations, on scales where the massive neutrinos free-streaming erase significantly their power spectrum (Lesgourgues & Pastor 2006), and is expected to be a key ingredient in pinpointing their total mass through global cosmological fits.

On statistical ground, the properties of the (nearly) optimal quadratic estimator for lensing power reconstruction are now well understood, both in the (infinite) flat sky limit and on the complete sphere (Hu & Okamoto 2002; Okamoto & Hu 2003).

However, real data are affected by contaminants, mostly galactic dust and point-sources for CMB frequency maps, and this requires reconsidering the strategy for lensing reconstruction on a cut-sky, which is a non-trivial task. Also, the scanning

strategy of the instrument, in particular in PLANCK, induces some strong spatial noise inhomogeneities, that are not taken into account in the classical estimator, and must be corrected for by Monte-Carlo simulations. In the general case, both effects will mix in the reconstruction process.

In a previous work (Perotto et al. 2010), we have optimized a sparse inpainting procedure to restore the missing data inside the mask, without biasing significantly the lensing results. We had however neglected the noise inhomogeneity. Furthermore, the work was oriented towards component-separated maps, so that the mask to be filled was rather small (about 10% of the sky).

But before having resort to a component separation method that mixes different maps, we wish to investigate in this paper whether the lensing potential can be reconstructed more directly on individual intensity CMB maps, which is anyway a necessary step in assessing possible systematic errors. For PLANCK the channels under consideration will be at 100, 143 and 217GHz (Planck Coll. 2005). This will require dealing with much larger masks and we will also take into account the strong spatial noise inhomogeneities induced by the scanning strategy.

We revisit the sparse inpainting method in this new configuration (a 30% mask + inhomogeneous noise) and will show that i) the estimator under these conditions is strongly biased, and ii) a Monte-Carlo approach can be used to correct from this bias. We propose also an alternative method (multi-patch) which

allows to avoid completely the galactic region, but requires to solve a number of issues related to the pixelized-sphere to plane projection.

After reviewing rapidly the various noise contributions to the quadratic estimator (QE) in Sect. 1, and the common simulations used in Sect. 2, we will update our full-sky inpainting analysis (hereafter denoted FS-inpainting) in Sect. 3. Most of the paper will then deal with solving issues related to the projection of a non-periodic signal from a pixelized sky onto a local patch, in Sect. 4. In particular, we present a new algorithm (detailed in the Appendix) that allows a fast reconstruction of band-limited Fourier series coefficients from irregularly sampled data, without performing any interpolation. We will then compare both methods, optimize the results in Sect. 5 and argue that a hybrid reconstruction is the most appropriate. In this hybrid approach, the full sky lensing reconstruction presented in (Perotto et al. 2010) is used at low ℓ , with an additive Monte-Carlo bias correction, while at high ℓ , the new multi-patch method is advocated.

This method allows the reconstruction of lensing directly on PLANCK-like CMB frequency maps (namely the 100, 143 and 217 GHz ones). While it would be premature to decide today whether performing a multi-map component separation is a better approach to lensing, we give some elements for the discussion in the conclusion.

1. A brief review of the quadratic estimator

The gravitational lensing potential ϕ is a scalar isotropic field (for a review, see *e.g.* Lewis & Challinor 2006) that *remaps* spatially the CMB photons according to

$$T(\mathbf{n}) = T_{\text{CMB}}(\mathbf{n} + \mathbf{d}(\mathbf{n})) \quad (1)$$

where $\mathbf{d} = \nabla\phi$ is the deflection field, which has a power spectrum on the sky $C_\ell^d = \ell(\ell+1)C_\ell^\phi$, or $C_K^d = k^2 C_K^\phi$ in the flat sky limit.

This process slightly breaks the gaussianity of the CMB field, and estimators has been searched for in order to extract the lensing information using its very local properties

The quadratic estimator has been proposed by Hu & Okamoto (2002). For CMB temperature anisotropies, it consists in taking the (weighted) convolution of the observed Fourier modes according to

$$\hat{\phi}(\mathbf{K}) = A_K \int \frac{d^2 k_1}{(2\pi)^2} T(\mathbf{k}_1) T(\mathbf{K} - \mathbf{k}_1) F(\mathbf{k}_1, \mathbf{K} - \mathbf{k}_1) \quad (2)$$

where the normalization A_K and filter F are determined demanding an un-biased estimator, and a minimal variance at the leading noise order (so-called $N^{(0)}$). For an idealized experiment, one gets:

$$A_K = \left(\int \frac{d^2 k_1}{(2\pi)^2} f(\mathbf{k}_1, \mathbf{K} - \mathbf{k}_1) F(\mathbf{k}_1, \mathbf{K} - \mathbf{k}_1) \right)^{-1} \\ F(\mathbf{k}_1, \mathbf{k}_2) = \frac{f(\mathbf{k}_1, \mathbf{k}_2)}{2C_{k_1}^{\text{tot}} C_{k_2}^{\text{tot}}} \quad (3)$$

where $f(\mathbf{k}_1, \mathbf{k}_2) = (\mathbf{k}_1 + \mathbf{k}_2) \cdot \mathbf{k}_1 \tilde{C}_{k_1} + (\mathbf{k}_1 + \mathbf{k}_2) \cdot \mathbf{k}_2 \tilde{C}_{k_2}$

The filter F involves on the numerator the CMB "true" unlensed power-spectrum (\tilde{C}_k), and on the denominator the "observed" one C_k^{tot} assumed to be a pure beam-deconvolved gaussian signal with un-coupled homogeneous noise.

Since this estimator involves only simple operations, it is computable in a few minutes on any standard computer. Its generalization to spherical harmonics on the full-sky has been performed in Okamoto & Hu (2003).

The full likelihood estimator has been worked out by Hirata & Seljak (2003), who have shown that it gives results very close to the quadratic one, given the current noise level, still involving much heavier computations.

The covariance of the $\hat{\phi}$ estimator is related to the true lensing potential spectrum C_k^ϕ through :

$$K^2 \langle \hat{\phi}(\mathbf{K})^* \hat{\phi}(\mathbf{K}') \rangle = (2\pi)^2 \delta(\mathbf{K} - \mathbf{K}') [K^2 C_K^\phi + N_K^{(0)} + \mathcal{O}(C_K^\phi)] \quad (4)$$

and remarkably, the noise term is directly related to the estimator normalization Eq. (3):

$$N_K^{(0)} = K^2 A_K \quad (5)$$

It corresponds to the *Gaussian* term, in the sense that it comes from the standard *disconnected* part of the four points correlator that appears when computing the noise and is therefore decoupled from the ϕ field. Equivalently, it represents the power of the QE when running it on unlensed maps.

A first order power spectrum correction term was soon discovered by Kesden et al. (2003). It comes from the *connected* part of the correlator, and therefore depends on the ϕ field itself: $N^{(1)}(\phi)$.

When actually coding the estimator for the PLANCK experiment, we still noticed an incomprehensible bias at low ℓ 's. It was finally tracked down by Hanson et al. (2010) to be a non-negligible second order term, that can be estimated analytically and was called $N^{(2)}(\phi)$. Another way to take this noise into account, is to use a simple "trick", due to P. Bielewicz, which consists in using the *lensed* spectrum in the numerator of Eq. (3). This approach has been shown to capture even more precisely the second-order contribution than the $N^{(2)}$ but slightly increases the error on the reconstructed signal.

This is however not the end of the story. Indeed, our simulations did not incorporate initially the spatial inhomogeneity of the noise, due to the PLANCK scanning strategy. This induces correlations between different Fourier modes, which lead to spurious signal reconstruction in the QE. It was shown in Hanson et al. (2009) that it affects the QE expectation value, and results in a low- ℓ bias in the power spectrum, which can be analytically estimated under the white noise hypothesis. However, this *mean field* approach still misses another $N_K^{(1)}$ -like term, which is non-computable analytically and affects the whole lensing spectrum.

Finally due to foregrounds, one can never have experimentally a signal on the full sphere. In that case, the spherical harmonics do not form anymore a "natural" basis and the issue of building a good estimator for lensing is non trivial. Even the inverse variance weighting of the map (*e.g.* (Smith et al. 2007)), a computationally very challenging task and sometimes referred to as being "optimal", will not provide an unbiased estimate of the lensing spectrum, because of the large modes coupling introduced by the mask and the inhomogeneous noise.

To take into account these last two effects, the treatment of the masked region and inhomogeneous noise, we add to the estimator covariance a $N_K^{\text{MC}}(\phi)$ term that can in general be dependent on the lensing field.

In summary, the deflection estimate variance from applying the QE on data using a given method, includes the following terms:

$$K^2 \langle \hat{\phi}(\mathbf{K})^* \hat{\phi}(\mathbf{K}') \rangle = (2\pi)^2 \delta(\mathbf{K} - \mathbf{K}') \cdot [C_K^d + N_K^{(0)} + N_K^{(1)} + N_K^{(2)} + N_K^{\text{MC}}] \quad (6)$$

where

- C_K^d is the seeked deflection spectrum
- $N_K^{(0)}$ is determined on the data given the knowledge of the underlying true power spectrum
- $N_K^{(1)}$, and $N_K^{(2)}$ can be computed analytically. Since they depend on the searched field, one may need to setup an iterative determination. In our simulation, we just use the fiducial value to compute them.
- N_K^{MC} is the bias of the power spectrum estimator, that depends on the inhomogeneous properties of the noise and the way to deal with the Galactic contamination (and the coupling of both).

The desired properties of N_K^{MC} is of course to be low, still keeping the best variance for the estimator, and decoupled from the lensing field. In the following, we will study this term for two methods using a set of simulations with inhomogeneous noise and a large mask.

We will somewhat loosely switch to the multipole notation (ℓ) in the full-sky case, the formal connection being performed in *e.g.* Hu (2000). We recall that on a square patch of size $L \times L$, the discrete Fourier modes are located on a grid

$$\mathbf{k} = k_{i,j} = \Delta k \begin{pmatrix} i \\ j \end{pmatrix} \quad (7)$$

with $\Delta k = \frac{2\pi}{L}$ (≈ 35 for $L = 10^\circ$), and (i, j) being integers. In these units the power spectrum $C_{|k|}$ is equivalent to C_ℓ in the flat sky limit (White et al. 1999).

2. Simulations

To evaluate the performance of our algorithms we build a set of realistic PLANCK-like frequency maps, *i.e.* a combination of all channels of a given frequency. The experimental characteristics are the ones published in Planck HFI Core Team et al. (2011) corresponding to almost 10 months of data-taking.

The most interesting channels for CMB analyzes in PLANCK, are the 100, 143 and 217GHz ones, where the galactic dust contamination increases with frequency but is still subdominant and other galactic foregrounds emissions (such as synchrotron or free-free), decreasing with the frequency band, are already weaker than the CMB (Planck Coll. 2005). The resolution of the instrument, which is crucial to the lensing reconstruction, goes however in the other direction with an average FWHM of the scanning beams of about 9.5', 7.1' and 4.7' respectively (Planck HFI Core Team et al. 2011). We have chosen to focus on the 217 GHz channel, because it is the most challenging one for lensing since it requires the largest galactic mask.

We have thus developed the following pipeline for our simulations:

We start with a Λ CDM cosmology $\{H_0 = 72, \Omega_b h^2 = 0.023, \Omega_{CDM} h^2 = 0.11, Y_{He} = 0.24, N_{eff} = 3.04, \tau = 0.09, n_s = 0.96, A_s = 2.4 \times 10^{-9}\}$, which is consistent with the WMAP 7-year best fit model (Larson et al. 2011), and run the Boltzmann code CAMB¹ to produce the corresponding spectra of CMB intensity/polarisation anisotropies and lensing potential, using Halofit (Smith et al. 2003) for non-linear corrections. Both lensed/unlensed spectra are computed by the code. In the following we just focus on temperature maps since this is the best-suited observable for reconstructing lensing in a PLANCK-like case.

These spectra then feed the LensPix² code, which provides a full-sky high resolution map in the HealPix³ scheme ($n_{side} = 2048$). We use a cutoff $\ell_{max} = 3000$ and checked that the resultant lensed spectrum is in excellent agreement with the theoretical ones, up to $\ell \lesssim 2750$, which is largely sufficient for our analysis. 100 realizations of such maps has been produced. We will refer to these maps (supposed to represent the data) as the H_1 set (*i.e.* lensed).

Starting from the CAMB lensed power spectra, we also produced 100 Gaussian realizations using the standard HealPix tools (namely `synalm_cxx/alm2map_cxx`) which will help us in de-biasing the lensing power spectrum estimate. We will refer in the following to these maps as the H_0 set (*i.e.* unlensed).

All maps have been smoothed by a 4.7' Gaussian beam using HealPix standard tools.

The noise on the maps is generated according to the characteristics measured in Planck HFI Core Team et al. (2011). More precisely, the 217 GHz colored noise power is used to generate an homogeneous Gaussian noise realization, that is then weighted in real space according to its (inverse) hit map. 100 of such maps has been produced and added to the previous ones. We then apply a 30% mask to remove the dust contamination in the Galactic plane.

Since it is not the scope of this study to investigate the systematics related to point source residuals, we assume that a point source mask with a perfect completeness is available. We build it by combining the PLANCK Early Release Compact Source Catalog of point sources detected in the 143, 217 and 353 GHz channels and including Sunyaev-Zel'dovich clusters (ESZ) and dust cold cores (CC) (Ade et al. 2011b,a,c), the WMAP 7-year catalog of point sources with a positive flux in the W band (Gold et al. 2011) and a catalog of IRAS/2MASS IR sources whose flux at 100 μm is above 2 Jy (Beichman et al. 1988; Jarrett et al. 2001). Each catalog entry is masked by a $5\sigma \approx 10'$ radius disk. This mask covers $\approx 1.7\%$ of the sky out of the galactic plane. When combining it with the Galactic one, we are left with a fraction $f_{sky} = 0.69$ of the sky.

Figure 1 shows one of this simulated map.

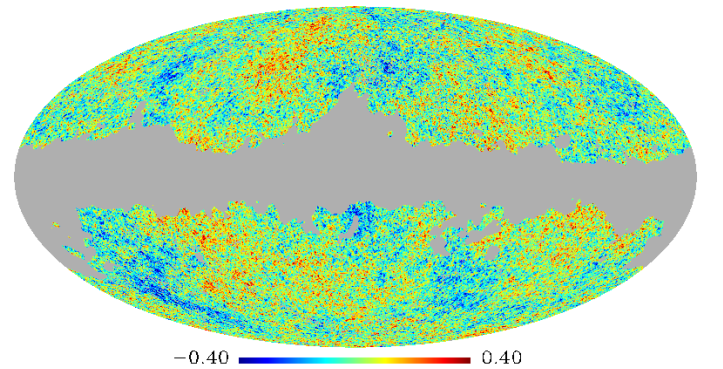


Fig. 1. Example of one of our simulated lensed temperature map, using the procedure described in the text. Units are mK_{CMB} . The gray region corresponds to the galactic mask that will be used. A point source mask is also included, but barely visible. It is more clearly seen on Fig 5.

² <http://cosmologist.info/lenspix>

³ <http://healpix.jpl.nasa.gov>

¹ <http://camb.info>

3. Update on the FS-inpainting method

In Perotto et al. (2010) we have studied the impact of an inpainting method to fill in, with an appropriate statistical mixture, a rather small mask (cutting a $\approx 10\%$ fraction of the sky). It was oriented toward component-separated maps, where such a level of final masking is to be expected. Here, we are pushing the algorithm harder by studying the filling of the large mask defined in Sect. 2 ($\approx 30\%$ of the sky). Furthermore, we add the spatially inhomogeneous noise, what will certainly affect the results of the algorithm.

We found that the inpainting algorithm implemented within the Multi-Resolution on the Sphere (MRS) package⁴, and based on spherical harmonics L_1 norm minimization using wavelet packet variance regularization (Abrial et al. 2007, 2008), provides the most robust results.

Each map from the H_0 and H_1 sets have been inpainted with it. An example of a restored map is shown on Fig. 2.

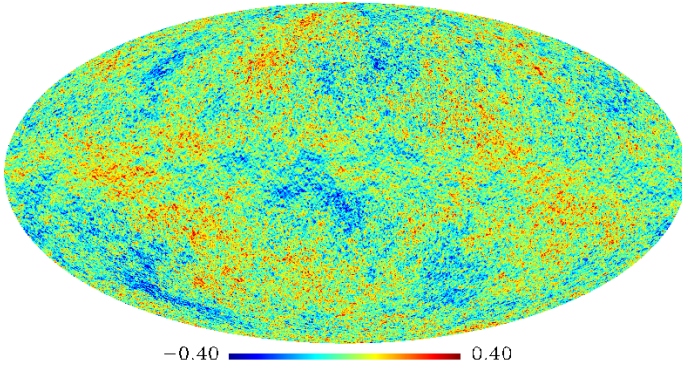


Fig. 2. Inpainted map corresponding to filling the galactic+point source mask of Fig 1.

We then apply the Hu&Okamoto quadratic estimator on the full-sky, using the fast spherical harmonic computations provided by the HealPix package, with a multipole cut $\ell_{\max} = 2000$, since there is no statistical gain in going to higher values given the noise level. The "observed" temperature spectrum that enters the QE filter is estimated on each map, which is a way of "absorbing" the residual spectrum deformation after the mask restoration. We did not use the Bielewicz's trick and therefore put the theoretical unlensed spectrum, as a numerator of the QE filter. Given the resolution and noise, we also computed analytically the $N^{(1)}$ and $N^{(2)}$ terms using the fiducial lensing power spectrum.

The bias size can then be estimated either on the H_0 or the H_1 simulations. In the former case, one directly measures a bias, after $N^{(0)}$ subtraction, that by construction, does not depend on the potential field. In the latter case, one can estimate the bias *w.r.t* to the fiducial model, after the $N^{(0)}, N^{(1)}, N^{(2)}$ corrections have been applied, that can grab some extra contributions. We want to check the robustness of our correction to the lensing field, by estimating N^{MC} on the H_0 set. The inpainting process is expected to induce a non-zero lensing coupled bias, since it cannot manage to thoroughly restore the lensed signal statistic up to the 4-point correlation function into the masked region.

However, this effect can be *effectively* accounted for by introducing an f_{sky} factor to correct for the lack of power due to the un-restored lensing modes within the mask, so that the QE variance reads:

$$\ell(\ell+1)\langle\hat{\phi}_{\ell m}^*\hat{\phi}_{\ell' m'}\rangle = \delta_{\ell\ell'}\delta_{mm'}(f_{\text{sky}}C_{\ell}^{\text{d}} + N_{\ell}^{\text{dd}}),$$

$$\text{where } N_{\ell}^{\text{dd}} = N_{\ell}^{(0)} + f_{\text{sky}}(N_{\ell}^{(1)} + N_{\ell}^{(2)}) + N_{\ell}^{\text{MC}}, \quad (8)$$

and the various contributions are shown on Fig. 3.

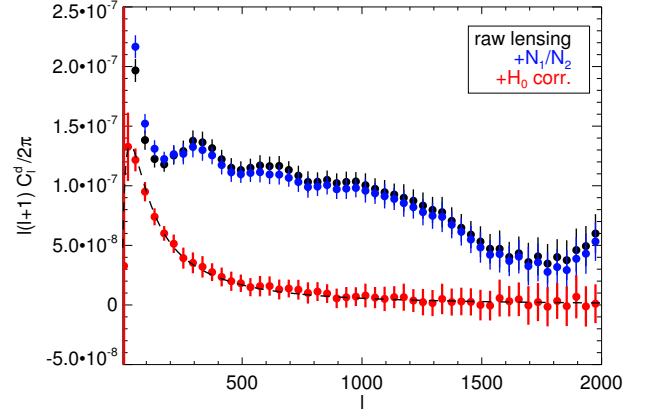


Fig. 3. Mean deflection spectra reconstructed with the FS-inpainting method on the lensed maps. "Raw lensing" denotes the spectrum reconstructed directly on the maps. In blue, is shown the effect of adding the (known) analytical terms $N^{(1)}$, $N^{(2)}$. In red, one further adds the Monte-Carlo correction obtained from the set of unlensed maps. The dashed line is the true input spectrum. All points are assigned an error bar corresponding to the variance of the Monte-Carlo's per sky map.

The bias of the estimator is quite important but corrected for by using the *unlensed* simulations. This means that the correction does not couple significantly to the lensing spectrum. It however still introduces *systematic* uncertainties related to a necessarily imperfect Monte-Carlo. This motivates the development of an alternative method which completely avoids the masking issue, to the price of introducing some new technicalities.

4. The local approach: multi-patch

Let us start with a simple example. How do you compute the power spectrum on a vector of sampled data?

1. one solution is performing the FFT in one shot: this gives many modes that can be averaged (binned) later on.
2. if you don't need too low frequencies, a solution is to slice your sample into bunches, apodize each one, perform the individual FFTs and take their mean.

Which one is better? It was found that using the second one, with overlapping chunks of data (by $\approx 50\%$) provides the nicest (binned) estimates (Oppenheim & Schaffer 1975). This is known as the Welch periodogram. Now what does happen if some portion of the data is missing? In the first case, one tries to *correct* for the gaps, possibly by restoring a mixture that has the right statistical properties given some prior for the signal, *i.e.* by performing an inpainting. It is much simpler in the multi-bunch case, where one just does not use chunks that overlaps with the

⁴ <http://jstarck.free.fr/mrs.html>

gaps, which is efficient as long as there are little of them and largely contiguous.

In the following we apply these ideas to the case of data located on a cut-sphere. We are going beyond the power spectrum estimation (that has been largely studied in Das et al. (2009)) and investigate whether this simple idea can be applied to CMB lensing reconstruction. In this case the main "gap" is the galactic plane and the "bunches" will be some tangent square planes.

We have thus developed a pipeline that allows for a local reconstruction of the CMB lensing on patches. It has the obvious advantage of avoiding the masked regions and should not introduce therefore the large bias due to the mask correlations that appears in any full-sky analysis. Furthermore, the noise inhomogeneity, which adds a sizable contribution to the lensing deflection, is also reduced by working locally.

Working spatially also allows us to inspect easily the quality of the data in different regions of the sky constraining experimental systematics. The natural flat sky formalism that will be applied can be easily interpreted, and indicators, as one for lensing isotropy, build.

Statistically, after determining the Fourier complex coefficients on each patches, we will use the Hu-Okamoto quadratic estimator (QE) described in Sect. 1. It has, by construction, a minimum variance (just as on the full-sky) so there is no statistical loss using this approach. However, obviously, no scales below the patch Fourier size $\frac{2\pi}{L}$ can be reconstructed, so we will miss the low multipoles.

4.1. Tiling the cut-sphere with patches

The first question to ask is what the typical size ($L \times L$) of the patches must be for lensing. It turns out to be a compromise between several considerations:

1. lensing correlates modes over a few degrees scale
2. the Fourier modes we will reconstruct being harmonics of $\frac{2\pi}{L}$ we prefer having a large L value to sample correctly the Fourier space.
3. when projecting data from the sphere onto the local tangent plane (using a gnomonic projection), we wish to avoid too much distortion, which requires not going to too large L values. The classical $L \lesssim 20^\circ$ upper limit for the flat sky approximation (White et al. 1999) has been derived from power spectra considerations and is not necessarily valid for the four points statistics we are considering in lensing.
4. a last aspect is related to the efficiency of tiling a given cut-sky with patches, which requires them to be small. Also, inspired by the Welsh periodogram, we are seeking for a configuration where the patches overlap by about 50%, so that there is a clear interplay between the patches center position and their size.

A good trade-off is obtained with patches of angular size $L \simeq 10^\circ$. As a simple tiling strategy, we locate them at the centers of an HealPix $n_{\text{side}} = 8$ map pixels, so we start with $12n_{\text{side}}^2 = 768$ patches. Then, only patches that do not intersect the Galactic mask are kept, which leaves 395 of them, covering a fraction $f_{\text{sky}} = 55\%$ of the sky (as represented on Fig. 4). In this configuration, the overlap (the mean number of patches a point of the sphere belongs to) is of $\simeq 1.7$.

4.2. Preparing the patches

Local point source inpainting. Before extracting the Fourier coefficients, we need to remove bright sources from the patches,

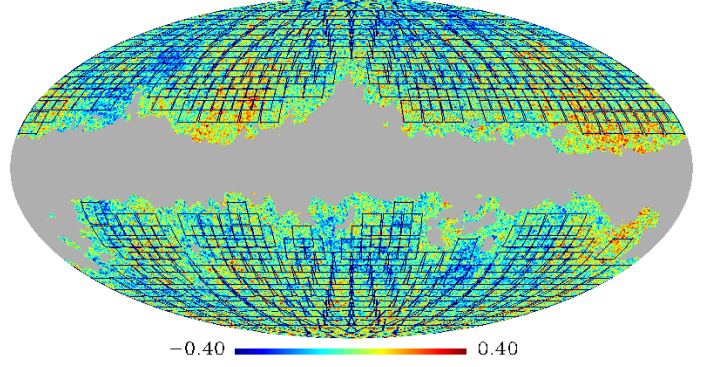


Fig. 4. Example of the tiling of the map shown on Fig. 1 with overlapping $10^\circ \times 10^\circ$ patches, that do not intersect the Galactic masked region.

which are a strong lensing contaminant. This is performed by using the point-source mask and filling the masked values by an inpainting algorithm, that is different from the one reported in Sect. 3. Indeed to keep the local nature of the whole analysis, so that each patch analyzed is independent of the others, we use a method that has been designed and tuned for weak lensing surveys FastLens⁵, which consists in minimizing the sparsity of DCT (Discrete Cosine Transform) coefficients for 256×256 data blocks.

More precisely, we construct high resolution regular images from the patches using bi-linear interpolation. The FastLens code is then run to fill in the point source masked areas. Then, the inpainted values are back-projected onto the sphere. When points fall in more than one patch, we use the inpainted values from the patch whose center is the closest, in order to avoid border effects.

This procedure is applied on the full set of H_0 and H_1 simulations. An example is shown on Fig. 5

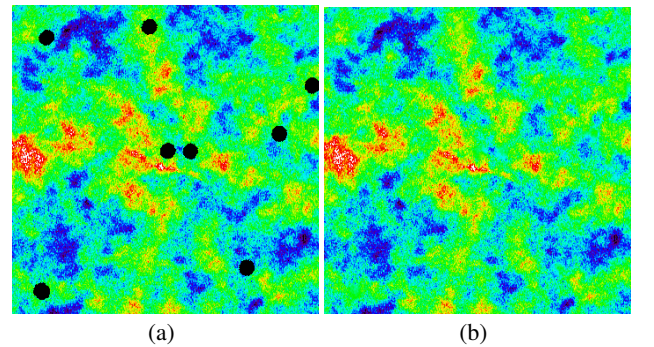


Fig. 5. (a) Example of a $10^\circ \times 10^\circ$ patch with masked sources in black. (b) Inpainting of the sources using the FastLens algorithm.

Prewhitening and apodization. At this stage, we could project the pixels onto patches, using a gnomonic projection, and reconstruct the Fourier coefficients (details in Sect. 4.3). However we

⁵ <http://irfu.cea.fr/Ast/fastlens.software.php>

noticed that the bi-dimensional temperature power-spectra obtained on these patches exhibit a strong leakage along the null Fourier axis (Fig. 6(a)).

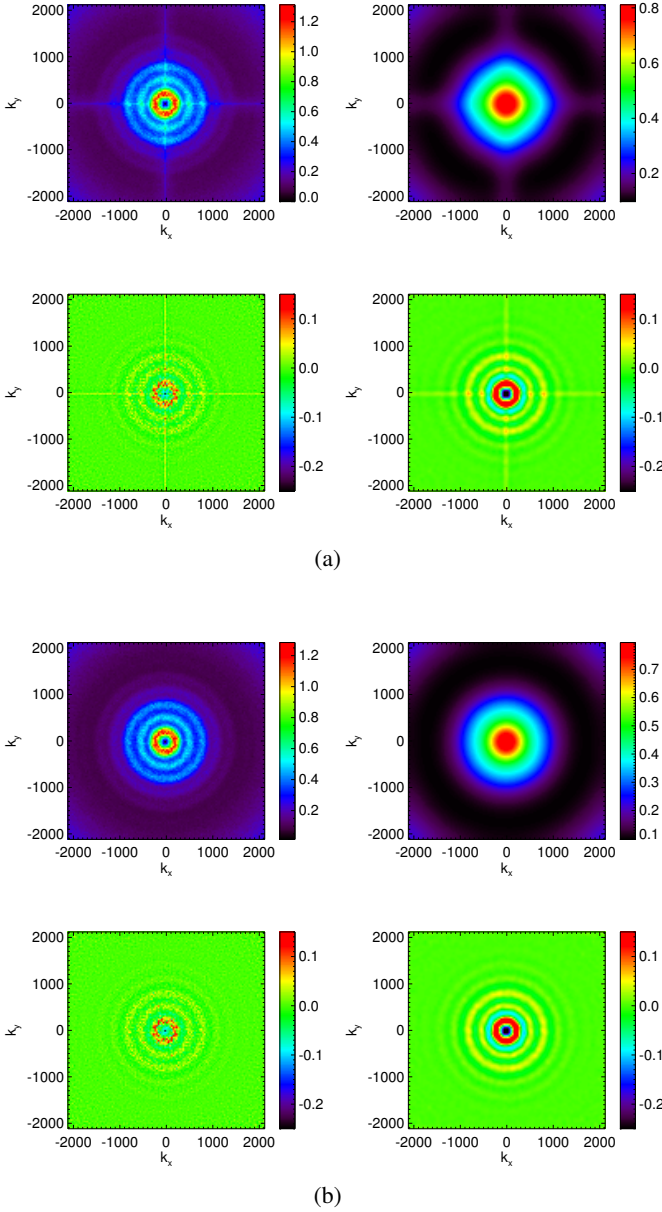


Fig. 6. (a) Bi-dimensional Fourier spectra of one of our simulation at different scales. Upper-left: mean of the squared-amplitude of the Fourier coefficients for all patches *i.e.* $k^2 \langle |a_{k_x, k_y}|^2 \rangle$. An isotropic un-decimated wavelet transform (“*a trous*”, see *e.g.* Starck & Murtagh (2010)) is applied to the image and the results for scale one and two are shown on bottom plots. The upper-right one corresponds to the smooth component. One notices a clear leakage along the null axes. (b) Same spectra but working on the prewhitened map and applying a Kaiser-Bessel $K_{0.5}$ window function. The leakage along the null axis has clearly disappeared.

We traced it to be due to the leakage of the low (k_x, k_y) modes, which have the stronger amplitudes, originating from the side-lobes of the implicit $10^\circ \times 10^\circ$ top-hat window used.

Instead of using some anisotropic filtering (the lensing itself being a source of anisotropy), we can correct this by *prewhitening* the map and applying an explicit window. Prewhitening is a standard ingredient in getting comparable size Fourier coefficients (*e.g.* Das et al. 2009). Since we are interested in a range up to $\ell \approx 2000$ (*i.e.* not too far into the damping tail), we need to approximately scale the spectrum by ℓ^2 . Even though we work on local patches, we have globally information above the typical Fourier scale, since we have a tiling of a large area of the sphere. Therefore, we simply multiply the map spherical harmonic coefficients by ℓ , and go back into direct space. In this process, the Galactic values are replaced by zero’s, which may slightly mix the mask into the data, but as will be checked on the Monte-Carlo this effect on lensing appears to be negligible. In the following we will work on these prewhitened maps for which the Fourier coefficients will be of similar order.

Rather than using the implicit top-hat window (with large side-lobes), we apply an explicit window to each patch in the direct space. We work with the family of Kaiser-Bessel functions (Kaiser 1966) which allow to vary simply the side-to-main lobe ratio, and that is still close to the optimal solution of energy concentration provided by the Discrete Prolate Spheroidal Sequence (Slepian 1978; Das et al. 2009).

Each value in the $L \times L$ size patch is therefore multiplied by:

$$W_\alpha(x, y) = W_\alpha^{(1)}(x)W_\alpha^{(1)}(y) \quad (9)$$

$$W_\alpha^{(1)}(x) = \frac{1}{I_0(\pi\alpha)} I_0\left(\pi\alpha \sqrt{1 - \left(x/\frac{L}{2}\right)^2}\right) \quad (10)$$

where I_0 denotes the zero-th order modified Bessel function of the first kind.

The Fourier transform of these windows is ⁶

$$\begin{aligned} \tilde{W}_\alpha(k_x, k_y) &= \tilde{W}_\alpha^{(1)}(k_x)\tilde{W}_\alpha^{(1)}(k_y) \\ \tilde{W}_\alpha^{(1)}(k_x) &= \frac{L}{I_0(\alpha\pi)} \text{sinc}\left(\sqrt{\left(\frac{k_x L}{2}\right)^2 - (\alpha\pi)^2}\right) \end{aligned} \quad (11)$$

which exhibits how the windows shrinks with α when comparing it to the tophat window in Fourier space: $\tilde{W}^{(1)}(k_x) = \text{sinc}(\frac{k_x L}{2})$.

We compute numerically the radial power of these windows as :

$$\begin{aligned} P_W(r) &= \frac{1}{2\pi} \int_0^{2\pi} |W_\alpha(r \cos \phi, r \sin \phi)|^2 d\phi \\ P_{\tilde{W}}(k) &= \frac{1}{2\pi} \int_0^{2\pi} |\tilde{W}_\alpha(k \cos \theta, k \sin \theta)|^2 d\theta \end{aligned} \quad (12)$$

and show them for $\alpha = 0.5, 1, 2$ on Fig. 7 in direct and Fourier space.

As is well known, diminishing the side-lobes is always to the price of increasing the main beam width (energy conservation). In the following, we want as small an α as possible to keep the window well peaked since the QE will take the products of modes that will be convolved by this window in Fourier space (Sect. 4.5).

We checked that after prewhitening and windowing with the Kaiser($\alpha = 0.5$) window, the power spectrum leakage disappears as is clear on Fig. 6(b). In the following we will therefore use $W_{0.5}$ as an explicit apodization function.

The size of the window in Fourier space, Fig. 7(b), fixes the binning. For $W_{0.5}$ on a $L = 10^\circ$ square patch, we use a step of $\Delta k = 40$, starting from the first available Fourier mode $k_0 = 35$,

⁶ In Eq. (11) a complex continuation is to be understood for low k_x values

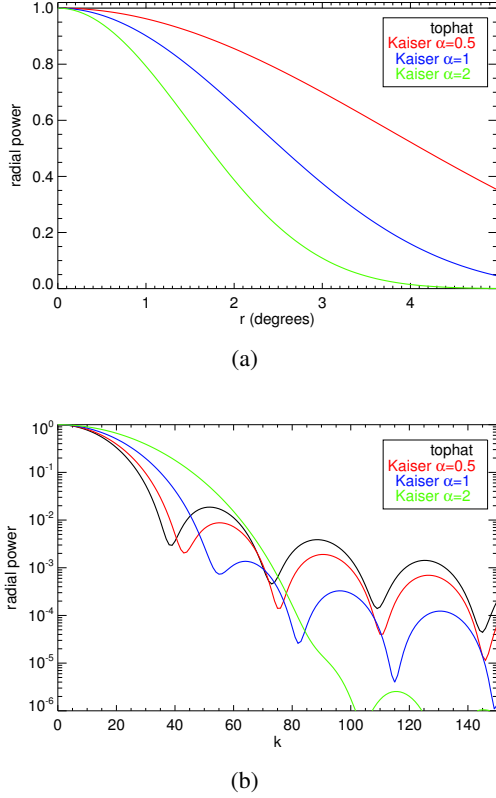


Fig. 7. Radial power of the Kaiser-Bessel 2D windows with $\alpha = 0.5, 1, 2$ for $L = 10^\circ$ in real (a) and Fourier (b) space. The top-hat result is also shown.

4.3. Fourier series estimation of non-equispaced data

We project the prewhitened map onto the local patches, using a gnomonic projection. The HealPix pixel centers then fall onto an irregular bi-dimensional grid. Can we still perform a spectral analysis?

For a $n_{\text{side}} = 2048$ HealPix map, the mean inter-pixel separation is about $1.7'$, which is *not* negligible compared to the expected mean deflection of the CMB lensing ($\approx 2.7'$), so that an interpolation would induce some large effects.

There exists some smart techniques to compute the NDFT, Discrete Fourier Transform of Non-equispaced data (Keiner et al. 2009) but they rather put accent on rapidity, in particular for multi-dimensional problems, by using a trade-off between speed and accuracy. Here we want to keep the maximal accuracy within a "reasonable" time. We have thus implemented, and generalized to two dimensions, the so-called "ACT" (Adaptive weight, Conjugate gradient, Toeplitz matrices) algorithm (Feichtinger et al. 1995) which performs a *least-squares fit* of the complex Fourier coefficients $a_{k,h}$ in the series expansion:

$$T(x, y) = \sum_{k=-M_x}^{M_x} \sum_{h=-M_y}^{M_y} a_{k,h} e^{2\pi i k \frac{x}{L}} e^{2\pi i h \frac{y}{L}} \quad (13)$$

In the general case, the brute force inversion of the normal equations is prohibitive, but the method takes advantage of the peculiar structure of the Fourier series decomposition (see Appendix). In our case, we determine the 120×120 coefficients from the $\approx 120\,000$ data values contained in a $10^\circ \times 10^\circ$ patch of an HealPix $n_{\text{side}} = 2048$ map, in about a minute on a standard computer.

This tool, named *FourierToeplitz*, has been compared to a standard FFT method, when fitting (actually solving) $N \times N$ points with $N \times N$ unknown on a *regular* grid: results agree within machine precision.

Since this is a fitting procedure (not an N to N mapping as in an FFT), the energy conservation (Parseval equality) is not imposed and we did not observe any aliasing effect.

Such a tool opens the road to local analyzes of projected spherical maps that are plagued by interpolation issues. It has already been used successfully in computing the spectra and full CMB bi-spectra in Pires et al. (2012).

4.4. Local power spectra estimates

After running the *FourierToeplitz* tool, we have an estimate of the complex Fourier coefficients per patch, at wavevector \mathbf{k} , located on the regular grid Eq. (7).

By computing the squared-amplitude map, one can study the 2D local power spectrum on the sky, and even though the cosmic variance is large, detect potential experimental problems. By taking the mean of all the patches power spectra, one can check for the CMB field isotropy in a simple way.

By plotting the values, *w.r.t* $|\mathbf{k}|$ (*i.e.* assuming isotropy) one constructs a 1D power spectrum, equivalent to the famous C_ℓ but on the non-integer values $|\mathbf{k}|$ given by Eq. (7). One has a powerful local power-spectrum estimator that solves the issues of masking that is well suited to jackknife tests. In order to get to a full determination of the spectrum, one would still have to study the window function, as in Hivon et al. (2002); Das et al. (2009), but we do not actually need it for the lensing reconstruction since it relies on the *observed* spectrum. We need first to deconvolve the maps from the beam, which is a trivial operation in Fourier space for a Gaussian lobe, and obtain some smooth spectrum. This is obtained by taking the mean power spectrum of the de-convolved Fourier patches, and fitting the coefficients of a generic smooth function to all the data points as explained in Plaszczynski & Couchot (2003). The result is shown for one of our simulation, on Fig. 8.

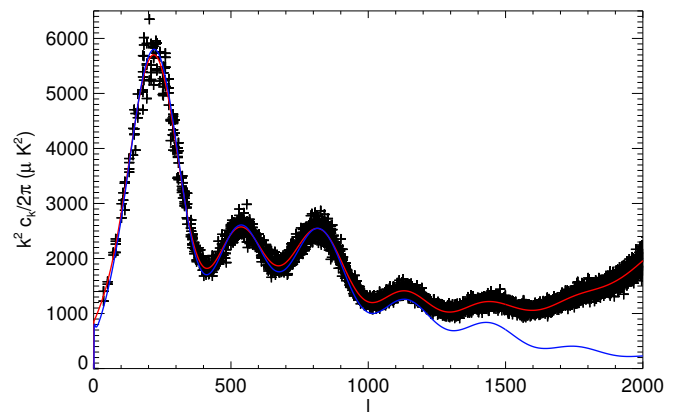


Fig. 8. Example of a 1D power spectrum used in the lensing estimator. The points are obtained from the bi-dimensional spectrum (as on Fig. 6(b)), de-convolved from the beam and represented *w.r.t* to $|\mathbf{k}|$. They are fitted to a smooth function in red. Also shown in blue is the fiducial model.

4.5. Local deflection estimates

Now that we have the complex Fourier coefficients for each patch, and the observed/true C_ℓ 's, we may apply exactly the Hu&Okamoto flat-sky estimator to obtain the (noisy) potential maps in the Fourier domain, Eq. (2). But before going on to the lensing spectrum estimate, we need to review the noise of the estimator on an *apodized* patch since the standard QE has not been derived for this case.

The quadratic term $\langle T(\mathbf{k}_1)T(\mathbf{K}-\mathbf{k}_1) \rangle$ over which is build the estimator Eq. (2) is affected in a non-trivial way by the apodization procedure. Metcalf & White (2007, Appendix B) show that it introduces:

1. an "aliasing" effect due to the overlap of the windows in Fourier space that will just affect the low ℓ 's modes.
2. some complicated "smoothing" of the lensing potential.

We do not try to build an optimal estimator from the elaborate expression. Instead we notice that the apodization process scales the lensing Gaussian noise by a merely constant factor, that can be understood in the following way.

Following closely on Hivon et al. (2002); Efstathiou (2004) one can show, that, assuming the window is well peaked in Fourier space so that the spectrum does not vary too much over it, the two-points correlation function of an apodized Gaussian field T^{apo} along with its variance can be approximated by

$$\langle T^{\text{apo}}(\mathbf{k}_1)T^{\text{apo}}(\mathbf{k}_2) \rangle \simeq (2\pi)^2 \delta(\mathbf{k}_1 + \mathbf{k}_2) w_2 C_{k_1} \quad (14)$$

$$\text{var}(T^{\text{apo}}(\mathbf{k}_1)T^{\text{apo}}(\mathbf{k}_2)) \simeq 2w_4 C_{k_1} C_{k_2} \quad (15)$$

where

$$w_i = \frac{1}{L^2} \int_{-L/2}^{L/2} \int_{-L/2}^{L/2} dx dy W^i(x, y) \quad (16)$$

and $W(x, y)$ is the window function in direct space.

These approximations are accurate for large k values (Efstathiou 2004) which corresponds, given our windows size to $k \gtrsim 100$.

In the following, we use windows normalized by $\sqrt{w_2}$, so that the reconstructed power spectrum, the only entity that varies with apodization in the filter/normalization of the QE, Eq. (3), is mainly unchanged (Eq. (14)). We checked for instance that applying a $W_{0.5}$ window does change the lensing normalization A_k by less than 1%.

The Gaussian noise in the apodized case can be written as the variance of the QE applied on the apodized *unlensed* sky:

$$N_K^{(0, \text{apo})} = K^2 \langle |\hat{\phi}^{\text{unlens, apo}}(\mathbf{K})|^2 \rangle. \quad (17)$$

Ingesting Eq. (15) into this equation and using the normalized window, one obtains

$$N_K^{(0, \text{apo})} \simeq \frac{w_4}{(w_2)^2} N_K^{(0)} \quad (18)$$

What is the accuracy of this approximation? We ran the QE on the unlensed simulations, compute the mean lensing spectrum and compare it to the ideal case given by Eq. (5). The result on Fig. 9 shows that the ratio is indeed reasonably flat for values of $\ell \gtrsim 100$. Fitting the mean value of this ratio on the high ℓ region gives a result very close to the analytical value $\frac{(w_2)^2}{w_4} = 0.859$.

We performed the exercise with other windows too (Table 1). They all show an excellent agreement with the simple $\frac{(w_2)^2}{w_4}$ scaling factor.

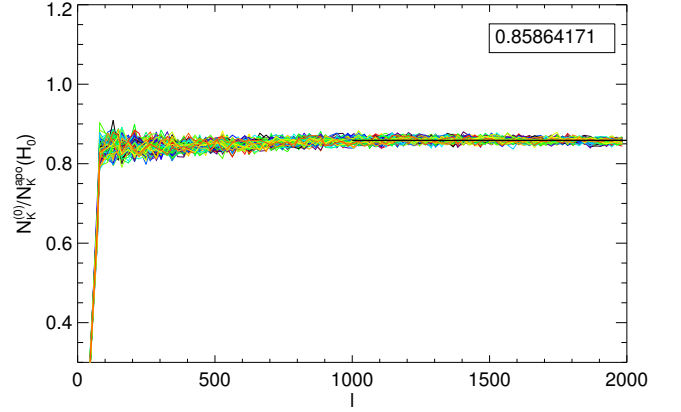


Fig. 9. Color plots shows the ratio between the non-apodized $N_K^{(0)}$ term Eq. (5) and the reconstructed lensing variance on the patches apodized by $W_{0.5}$ on each of the 100 maps of our unlensed (H_0) set. A constant term, whose value is depicted in the upper box, is fitted on the $\ell \geq 1000$ part.

| window | $\frac{(w_2)^2}{w_4}$ | MC- H_0 |
|--------------------------|-----------------------|-----------|
| Top-hat | 1 | 1 |
| Kaiser($\alpha = 0.5$) | 0.859 | 0.859 |
| Kaiser($\alpha = 1$) | 0.502 | 0.505 |
| Kaiser($\alpha = 2$) | 0.248 | 0.249 |
| Hanning | 0.264 | 0.265 |

Table 1. Comparison of the lensing excess Gaussian noise due to various apodization windows. $\frac{(w_2)^2}{w_4}$ is the analytical approximation, whereas the last column gives the measured ratio from the unlensed Monte-Carlo's, obtained as on Fig. 9. For completeness we also added the Hanning window result (Oppenheim & Schafer 1975).

This leads us to rewriting the QE total covariance Eq. (4) in the apodized case, as:

$$K^2 \langle \hat{\phi}(\mathbf{K})^* \hat{\phi}(\mathbf{K}') \rangle = (2\pi)^2 \delta(\mathbf{K} - \mathbf{K}') \cdot \frac{w_4}{(w_2)^2} [C_K^d + N_K^{(0)} + N_K^{(1)} + N_K^{(2)} + N_K^{\text{MC}}] \quad (19)$$

and propose the following simple estimator for an apodized patch:

$$K^2 \widehat{C}_K^\phi = \frac{(w_2)^2}{w_4} \int \frac{d\phi}{2\pi} K^2 |\hat{\phi}^{\text{apo}}(\mathbf{K})|^2 - (N_K^{(0)} + N_K^{(1)} + \dots) \quad (20)$$

where the integral is performed in small size rings over the discrete Fourier grid.

This *proposed* estimator, Eq. (20), will then be tested on our H_1 simulations in order to assess its bias/variance. It is worth noticing that the value of the scale factor does not need to be known very precisely. What cares, is that the *same* factor be used on the data (here H_1) and the Monte-Carlo correction (here H_0).

We now have all in hands to compute the deflection power-spectra. This is performed for each map of our Monte-Carlo set, in the following way:

1. From the Fourier coefficients obtained on each patch, form the 2D-Fourier potential map $\hat{\phi}$ using Eq. (2). The normalization (and $N_K^{(0)}$ term) is computed the standard way, Eqs. (5),(3) using the true/observed spectrum as on Fig. 8.

2. For each patch, form the noise corrected deflection power map from $fK^2|\hat{\phi}_K|^2 - N_K^{(0)}$ where $f = 0.86$ in our case.
3. Accumulate the 395 power maps, build their mean and variance.
4. Compute the inverse-variance weighted average in rings of constant $\Delta K = 40$ width (starting at $K_0 = 35$). The binned values will be reported at the mean of the different modes $K_{i,j}$ locations within the ring.

We compute these spectra on the H_1 set, which have still noise contributions from $N^{(1)}$, $N^{(2)}$ and N^{MC} terms. The N^{MC} term (the "bias") is taken from the H_0 simulations as the mean difference to 0 of the reconstructed spectra following the same procedure.

The mean spectrum is shown on Fig. 10, where one sees the various contributions.

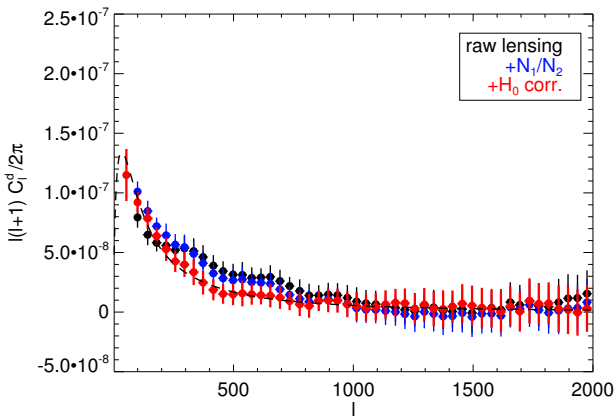


Fig. 10. Mean deflection spectra reconstructed by the multi-patch method on the lensed maps. "Raw lensing" denotes the spectrum measured directly on the maps as described in the text without performing any bias correction. In blue, is shown the effect of subtracting the (known) analytical terms $N^{(1)}$ and $N^{(2)}$. In red, one further accounts for the Monte-Carlo correction obtained on the set of all unlensed maps. The dashed line is the fiducial input spectrum. All points are assigned an error bar corresponding to the variance of the Monte-Carlo's per sky map. The first bin for the raw-lensing estimate is located out of the plot (at a value of 3.5×10^{-7}). The same range as on Fig. 3 has been used for proper comparison.

The initial (raw) lensing spectrum estimate has already a very little bias, thanks to not using any galactic data and to a reduced local noise inhomogeneity.

We show that the multi-patch method leads, after a small correction, to an unbiased estimate of the deflection over the whole $\ell \in [75, 2000]$ range. The very first bin $[35, 75]$ is also unbiased but receives a stronger correction from the H_0 MC which is due to the breakdown of the flat-sky limit (ℓ cannot be anymore identified to $|k|$) and to the fact that the apodization window has an overlap integral which extends approximately to 100 (see Fig. 7(b)).

It is worth noticing that the fact that unlensed simulations corrects accurately the lensed ones means that *the full reconstruction process does not induce any (significant) couplings to the underlying lensing potential*. The variance of the estimator will be discussed in the next part.

Finally, note that working on patches has a number of other benefits:

1. we actually do have bi-dimensional maps of the lensing potential, so that similarly to Fig. 6, we can test the deflection field isotropy easily. An example is shown on Fig. 11.
2. for each patch, we can check for unexpected systematics effect that would provide an excessive lensing signal (as missed sources).
3. knowing the noises, one can Wiener-filter each patch to reconstruct the lensing potential maps that can then be cross-correlated to other cosmological probes of the matter, such as galactic weak lensing (Cosmic Shear) or Cosmic Infrared Background, that are generally measured only over a small region of the sky.

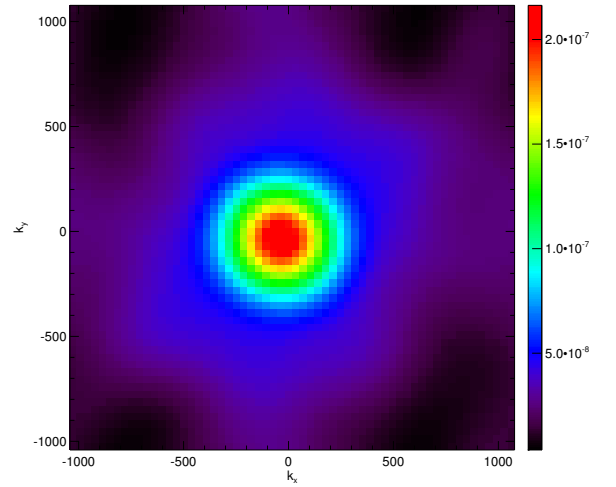


Fig. 11. Example of isotropy check of the lensing potential. For one of our lensed map, we build the "raw lensing" estimator (*i.e.* that does not include any MC correction) for each patch, and take their mean. We represent the power map $k^4 \hat{C}_k^\phi$ after $N^{(0)}$ subtraction, and smoothed by an "a trous" transform, as on the upper right part of Fig. 6(b).

5. Comparison of the methods

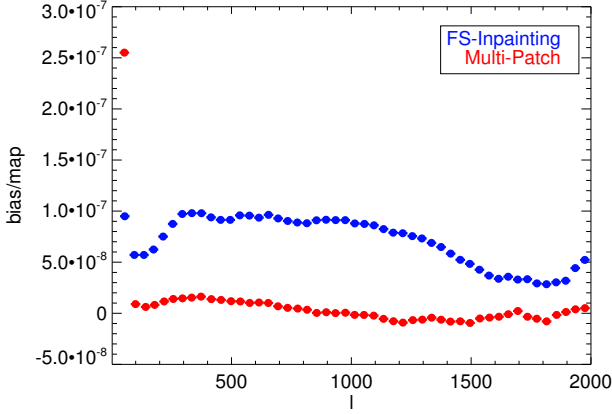
On Fig. 12 we compare the bias, in each ℓ bin, of the FS-inpainting and multi-patch methods. They have been obtained using *unlensed* simulations, and it was shown that they indeed correct the deflection power measure on lensed maps. We recall that the binning that has been used starts at $\ell = 35$ (first multi-patch accessible mode for a $10^\circ \times 10^\circ$ patches), with a width $\Delta\ell = 40$. Two extra bins have been added to FS-inpainting: $[2, 13]$ and $[14, 34]$.

The standard deviation in each bin from the H_1 set is shown on Fig. 13. The Fisher error estimate for the QE

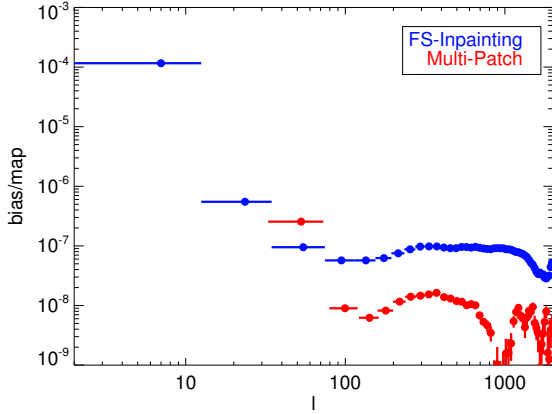
$$\sigma_\ell = \frac{C_\ell^d + N_\ell^{(0)}}{\sqrt{\ell \Delta\ell f_{\text{sky}}}} \quad (21)$$

is also depicted. We recall that the multi-patch method has a lower sky coverage ($f_{\text{sky}} = 0.55$) than the inpainted one ($f_{\text{sky}} = 0.69$) due to the procedure for tiling the cut-sky.

From these plots it appears that:



(a)



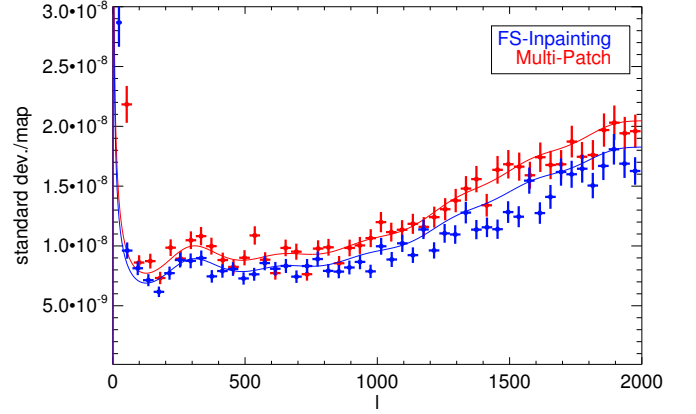
(b)

Fig. 12. (a) Bias of the methods computed from our simulations as the mean of the spurious deflection power on the unlensed set. For FS-inpainting, it corresponds to $N_\ell^{\text{MC}}/f_{\text{sky}}$ in Eq. (8) whereas for multi-patch, it is the result of applying the modified QE on H_0 (as described in Sect. (4.5)) (b) same plot with log scale to emphasize low ℓ 's. No mode below 35 is available to the multi-patch method.

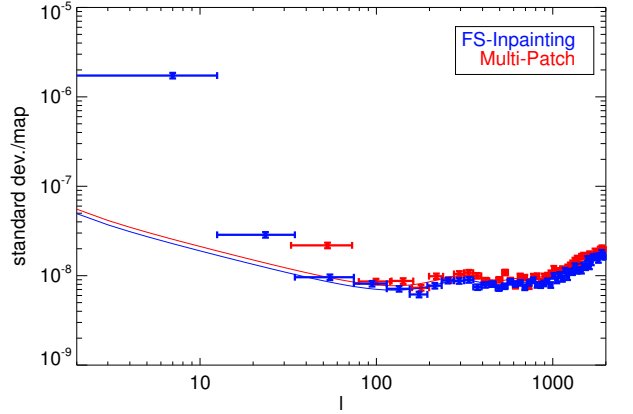
- The multi-patch approach shows clearly less bias, except for the very first bin [35, 75]. It cannot reconstruct modes below that values.
- in the large $\ell \gtrsim 100$ both estimators follow the naive Fisher error estimates, the FS-inpainting one having a slightly lower variance than for multi-patch, owing to a larger sky coverage.

We feel that the slight statistical loss ($\approx 10\%$) of the multi-patch method is largely compensated by the gain on systematic errors. As explained in Sect. 4, the reconstruction can be controlled at each step, visually inspected, but most importantly *the systematic errors due to the bias of a necessarily imperfect simulation is minimized.*

We therefore advocate the use of an hybrid method consisting in the multi-patch approach for $\ell \gtrsim 100$ and FS-inpainting for lower ℓ 's.



(a)



(b)

Fig. 13. (a) Standard deviation of the methods computed from our simulations, as the spread in each bin of the lensing estimators on the 100 H_1 set. (b) same plot with log scale to emphasize low ℓ 's.

Conclusion

We investigated two methods to reconstruct the lensing deflection power spectrum on PLANCK-like CMB frequency maps, using a large galactic cut and including some strong noise inhomogeneity. The first one, FS-inpainting, already presented in Perotto et al. (2010), is still found to be efficient in this severe configuration as long as one corrects for a large yet lensing-independent bias using Monte-Carlo's. We developed a new method well-suited in dealing with large masks, based on tiling the cut-sky with $10^\circ \times 10^\circ$ patches and performing local analyzes. This required to solve some issues related to non-periodic boundary conditions, and Fourier coefficients determination on irregularly sampled 2D data. To this purpose we have developed the FourierToeplitz tool, that allows the fast *exact* fitting of the Fourier series coefficients on irregularly sampled 2D data. This is a valuable tool to other analyzes that require a high level of precision on the spatial location.

Both methods have been intensively tested and compared on realistic PLANCK-like simulations of the 217 GHz CMB channel. It was found that the multi-patch approach has a very low bias in the whole $100 \leq \ell \leq 2000$ range, thanks to avoiding the galactic plane, and to lower local noise inhomogeneity.

It allows at each step, to check for experimental systematics errors and perform local images of both the temperature and deflection bi-dimensional power spectra. Its final variance is only marginally larger than a full-sky method, and could be improved by a smarter strategy for tiling the cut-sky sphere. The final result is not sensitive to the precise position of the patches, nor to the data overlap, since we obtain very similar results by using $12^\circ \times 12^\circ$ patches or other patch centers configurations. In order to perform some cosmological fits from the reconstructed spectrum, the inter-bin correlation would still have to be measured accurately, and included in the likelihood, since we observed some $(15 \pm 10)\%$ correlation level, with our $\Delta\ell = 40$ binning. This requires a large number of simulations (≈ 1000).

In the $\ell \leq 100$ range, we advocate using the FS-inpainting method that provides the minimal variance estimate on the cut sky.

These results open the road to measuring CMB lensing directly on PLANCK-like CMB maps, without even performing a component separation of the foregrounds. This is not exactly true for the FS-inpainting method, where one must have clean boundaries at the mask frontier. However this can be obtained by a simple template subtraction measured on the high frequency channels. For the multi-patch method, one can still perform the analysis without "un-dusting" the map, by choosing appropriate CMB dominated patches; we checked on simulations that a sub-dominant amount of dust contamination does not affect the lensing deflection spectrum.

It is not our goal to come to a decision on whether a component separation method is the better way to lensing reconstruction, since it is an area still under active development. Let us however notice that the statistical gain offered by using a larger fraction of the sky can be counterbalanced by an increased $N^{(0)}$ term due to a larger (combined) lobe of the instrument or a higher final noise level (see Eq. (21)). Also, adding the high/low frequency channels will "bring back" some additional infrared/radio sources that will need to be masked out, lowering the final statistical gain of the combined map.

Working directly on intensity maps allows to perform various sanity tests by checking the consistency between reconstructions from different frequency maps, which is a way to assess the robustness of the estimate against either experimental uncertainties or physical contamination – as from possible SZ-lensing or unresolved radio-sources-lensing correlations. The reconstructions on each frequency maps can also be minimum-variance combined, which offers a robust reconstruction that allows for a high level of systematics control. Finally, this is a well-suited approach to cross-correlation studies with other mass tracers, by selecting frequencies not affected by contaminants which may induce extra-correlations. For instance one may want to use only frequencies over 100 GHz (with negligible unresolved radio-sources contamination) while studying correlations with external radio surveys, or below 217GHz for a CIB-lensing correlation estimate.

Acknowledgements. We acknowledge the use of CAMB (Lewis et al. 2000), HealPix (Górski et al. 2005), LensPix (Challinor & Lewis 2005), MRS (Starck et al. 2006), FastLens (Pires et al. 2009) and FuturCMB2 (Perotto et al. 2006) packages. We thank Simon Prunet for the precise derivation of the effective number of degrees of freedom in Hivon et al. (2002) and Martin Reinecke for some dedicated HealPix C++ developments.

Appendix: FourierToeplitz tool

In order to not loose accuracy on the determination of Fourier coefficients from a sample of irregularly sampled points, we have developed a tool for *fitting* these coefficients in a reasonable time.

Let us start with the 1D case, where we implemented the "second generation" algorithm proposed in Feichtinger et al. (1995).

Let f be a function sampled on any support $\{t_i\}$. On a given interval $(0, T)$ the function can be expanded into a Fourier series:

$$f(t) = \sum_{k=-\infty}^{\infty} a_k e^{2\pi i k \frac{t}{T}}$$

Assuming that it has a band-limited spectrum, so that we can limit the number of Fourier modes to:

$$f(t) = \sum_{k=-M}^M a_k e^{2\pi i k \frac{t}{T}}$$

the problem is to determine the a_k coefficients given the sampled values f_i .

Let us work with the reduced $u = \frac{t}{T}$ variable. If the number of samples u_i is N , one writes the N equations

$$f_i = \sum_{k=-M}^M a_k e^{2\pi i k u_i}$$

This is a linear system of N equations with $2M+1$ unknowns. The well known normal equations obtained from least-squares minimization are:

$$(G^T G)X = G^T F$$

where F is the column vector of sampled values and G is the matrix with elements $g_{kl} = e^{2\pi i k u_l}$.

The solution is in general computationally heavy using standard methods.

Here, the interesting point is that the generic term of the system is of type:

$$T_{kl} = \sum_{j=1}^N e^{-2\pi i (k-l)u_j}$$

which is a Toeplitz matrix. One solves the system using the conjugate-gradient algorithm (the matrix is hermitian and positive) which consists in performing successive matrix-vector products. One then pads the Toeplitz matrix with zeros to obtain a circulant matrix, since the product of a circulant matrix with a vector can be computed efficiently using an FFT.

We have extended this method to the 2D case using the formalism of the Kronecker products of matrices and the properties of separability of FFTs. This allows for the fast determination of the a_{kh} coefficients in the Fourier expansion

$$f(x, y) = \sum_{k=-M_x}^{M_x} \sum_{h=-M_y}^{M_y} a_{kh} e^{2\pi i k \frac{x}{L_x}} e^{2\pi i h \frac{y}{L_y}}$$

In our case, a $10 \times 10^\circ$ patch from an HealPix $n_{\text{side}} = 2048$ map, contains about 120000 irregularly sampled values.

The modes are harmonics of $\Delta k_x = \Delta k_y = \frac{2\pi}{L} \approx 35$, so we need to determine 120×120 (half is negative) of them to obtain all modes below $l_{\text{max}} = 2000$. This is performed in about 1 minute on a single core. The conjugate gradient converges in about 7 iterations, without using any special pre-conditioner, so we did not add the adaptive weight scheme.

References

- Abrial, P., Moudden, Y., Starck, J., et al. 2007, *Journal of Fourier Analysis and Applications*, 13, 729
- Abrial, P., Moudden, Y., Starck, J.-L., et al. 2008, *Statistical Methodology*, 5, 289, arXiv:0804.1295
- Ade, P. A. R., Aghanim, N., Arnaud, M., et al. 2011a, *A&A*, 536, A8
- Ade, P. A. R., Aghanim, N., Arnaud, M., et al. 2011b, *A&A*, 536, A7
- Ade, P. A. R., Aghanim, N., Arnaud, M., et al. 2011c, *A&A*, 536, A23
- Beichman, C. A., Neugebauer, G., Habing, H. J., Clegg, P. E., & Chester, T. J., eds. 1988, *Infrared astronomical satellite (IRAS) catalogs and atlases. Volume 1: Explanatory supplement*, Vol. 1
- Challinor, A. & Lewis, A. 2005, *Phys. Rev. D*, 71, 103010
- Das, S., Hajian, A., & Spergel, D. N. 2009, *Phys. Rev. D*, 79, 083008
- Das, S., Sherwin, B. D., Aguirre, P., et al. 2011, *Physical Review Letters*, 107, 021301
- Efstathiou, G. 2004, *MNRAS*, 349, 603
- Feichtinger, H., Grochenig, K., & Strohmer, T. 1995, *Numer. Math.*, 69, 423
- Gold, B., Odegard, N., Weiland, J. L., et al. 2011, *ApJS*, 192, 15
- Górski, K. M., Hivon, E., Banday, A. J., et al. 2005, *ApJ*, 622, 759
- Hanson, D., Challinor, A., Efstathiou, G., & Bielewicz, P. 2010, *ArXiv e-prints*
- Hanson, D., Rocha, G., & Górski, K. 2009, *MNRAS*, 400, 2169
- Hirata, C. M. & Seljak, U. 2003, *Phys. Rev. D*, 67, 043001
- Hivon, E., Górski, K. M., Netterfield, C. B., et al. 2002, *ApJ*, 567, 2
- Hu, W. 2000, *Phys. Rev. D*, 62, 043007
- Hu, W. & Okamoto, T. 2002, *ApJ*, 574, 566
- Jarrett, T. H., Van Dyk, S., & Chester, T. J. 2001, in *Bulletin of the American Astronomical Society*, Vol. 33, American Astronomical Society Meeting Abstracts #198, 856
- Kaiser, J. F. 1966, In Kuo, F. F. and Kaiser, J. F. (Eds.), *System Analysis by Digital Computer*, chap. 7 (New York, Wiley)
- Keiner, J., Kunis, S., & Potts, D. 2009, *ACM Trans. Math. Software*, 36, 4
- Kesden, M., Cooray, A., & Kamionkowski, M. 2003, *Phys. Rev. D*, 67, 123507
- Larson, D., Dunkley, J., Hinshaw, G., et al. 2011, *ApJS*, 192, 16
- Lesgourgues, J. & Pastor, S. 2006, *Phys. Rep.*, 429, 307
- Lewis, A. & Challinor, A. 2006, *Phys. Rep.*, 429, 1
- Lewis, A., Challinor, A., & Lasenby, A. 2000, *ApJ*, 538, 473
- Metcalf, R. B. & White, S. D. M. 2007, *MNRAS*, 381, 447
- Okamoto, T. & Hu, W. 2003, *Phys. Rev. D*, 67, 083002
- Oppenheim, A. V. & Schaffer, R. W. 1975, *Digital Signal Processing* (Upper Saddle River, NJ, USA: Prentice Hall Press)
- Perotto, L., Bobin, J., Plaszczynski, S., Starck, J.-L., & Lavabre, A. 2010, *A&A*, 519, A4
- Perotto, L., Lesgourgues, J., Hannestad, S., Tu, H., & Y Y Wong, Y. 2006, *J. Cosmology Astropart. Phys.*, 10, 13
- Pires, S., Plaszczynski, S., & Lavabre, A. 2012, *Statistical Methodology*, 9, 71, special Issue on Astrostatistics + Special Issue on Spatial Statistics
- Pires, S., Starck, J.-L., Amara, A., et al. 2009, *MNRAS*, 395, 1265
- Planck Coll. 2005, *Blue Book* (ESA), available from <http://www.rssd.esa.int/planck>
- Planck HFI Core Team, Ade, P. A. R., Aghanim, N., et al. 2011, *A&A*, 536
- Plaszczynski, S. & Couchot, F. 2003, *ArXiv Astrophysics e-prints*
- Slepian, D. 1978, *The Bell System Technical Journal*, 57, 5, 1371
- Smith, K. M., Zahn, O., & Doré, O. 2007, *Phys. Rev. D*, 76, 043510
- Smith, R. E., Peacock, J. A., Jenkins, A., et al. 2003, *MNRAS*, 341, 1311
- Starck, J.-L., Moudden, Y., Abrial, P., & Nguyen, M. 2006, *A&A*, 446, 1191
- Starck, J.-L. & Murtagh, F. 2010, *Astronomical Image and Data Analysis* (Springer)
- Stompor, R. & Efstathiou, G. 1999, *MNRAS*, 302, 735
- White, M., Carlstrom, J. E., Dragovan, M., & Holzzapfel, W. L. 1999, *ApJ*, 514, 12